Cellular cryo-tomography of nidovirus replication organelles

Wolff, G.

CHAPTER 5

Conservation of a double-membrane spanning molecular pore in the replication organelles of distantly-related nidoviruses

Georg Wolff [1], Ronald W.A.L. Limpens [1], Anja W.M. de Jong [1], Abraham J. Koster [1], Eric J. Snijder [2], Montserrat Bárcena [1]

[1] Section Electron Microscopy, Department of Cell and Chemical Biology, Leiden University Medical Center, Leiden, The Netherlands.

[2] Molecular Virology Laboratory, Department of Medical Microbiology, Leiden University Medical Center, Leiden, The Netherlands.

In preparation for submission

Abstract

As coronaviruses and other nidoviruses studied so far, arteriviruses transform membranes of the infected cell into double-membrane vesicles (DMVs) that appear to be associated with viral RNA synthesis. These DMVs so far have been characterized as sealed compartments that would not allow the straightforward transfer of newly synthesized viral RNAs from their lumen into the cytosol. For the distantly related coronaviruses, the recently discovered molecular pore spanning both DMV membranes appears to provide a solution for this topological problem. However, structural and functional details of these pores, as well as the degree of conservation across the Nidovirales order remain unclear. Here, we used cellular electron cryo-tomography to study the DMVs induced by two prototypic arteriviruses and investigate their macromolecular details. We revealed that the DMVs induced by these arteriviruses also contain double-membrane spanning pores that appear to be involved in the transport and encapsidation of viral RNAs. In addition, the expression of two viral transmembrane proteins was found sufficient for the formation of double membrane-spanning pores. This demonstrates that as the presence of genomic RNA or the enzymatic machinery of the replication and transcription complex (RTC) is not required for pore formation. Our study illustrates the conservation of DMV molecular pores across two families of distantly related nidoviruses, which emphasizes their likely crucial role in the coordination of viral RNA synthesis and genome encapsidation.

Introduction

The order *Nidovirales,* which currently comprises 14 virus families, was initially established to unite the distantly related *Arteriviridae* and *Coronaviridae* (*1*), which share important similarities in terms of the organization and expression of their polycistronic positive-sense RNA (+RNA) genomes (*2*). While coronaviruses recently gained worldwide attention for being potentially lethal human pathogens, the family arteriviruses (thus far) contains only animal pathogens. The best-studied arteriviruses are the equine arteritis virus (EAV) and the porcine reproductive and respiratory syndrome viruses (PRRSV) 1 and 2, now formally classified within the species *Alphaarterivirus equid* and *Betaarterivirus suid 1* and *2*, respectively (https://talk.ictvonline.org/taxonomy/). Over the past decades, PRRSV in particular has had significant impact worldwide, causing major economic losses to the swine industry (*22*).

The complex evolutionary history of nidoviruses is highlighted by the fact that their genome size ranges from 12 to 41 kilobases (kb) (*37*), with arterivirus genomes being most compact at 12-16 kb. A conserved feature is the presence of two large 5'-proximal open reading frames (ORFs 1a and 1b) that are translated into the replicase polyproteins (pp) 1a and 1ab, the latter being a C-terminally extended version of the former that derives from ribosomal frameshifting. A common ancestry was postulated for an array of key functional domains in the replicase polyproteins (see Fig. 1 and (*119*)), which are the precursors of the nonstructural proteins (nsps) that drive RNA synthesis in the infected cell. On the other hand, despite all being enveloped virions, the size and morphology of nidovirus particles can vary widely. For example, whereas coronavirions are ~100 nm in diameter and well known for their prominent surface projections, arterivirus particles have a diameter of only 50-60 nm and a smooth envelope, due to the short ectodomains of their envelope proteins (*228, 229*).

In the case of arteriviruses, the pp1a and pp1ab replicase polyproteins are approximately 1,700-2,500 and 3,200-4,000 amino acids long, respectively. They are proteolytically cleaved by three to five ORF1a-encoded arterivirus proteinases, yielding 13-17 nsps, depending on the arterivirus species (*228, 229*). Most of these cleavage products are thought to assemble into RNA polymerase-containing protein complexes that direct genome replication and the production of an extensive set of subgenomic mRNAs (sg-mRNAs) in arterivirus-infected cells (*228, 229*). The latter serve to express the structural protein genes of arteriviruses.

To support the replication of their RNA genomes, all +RNA viruses of eukaryotes studied so far induce the formation of specialized membrane structures in the host cytosol (*41, 230*). In the case of nidoviruses, the main structural element of these so-called viral replication organelles (ROs) are double-membrane vesicles (DMVs). Studies on arteriviruses, especially on the family prototype EAV, contributed importantly to our understanding of the organization of nidovirus RNA synthesis in the infected cell and the importance of the ROs with which the process is associated (*51, 56, 231*). The DMVs are part of elaborate membrane networks derived from the endoplasmic reticulum (ER) (*55-57, 59*). Nonstructural proteins containing multiple transmembrane domains (TMDs), the ORF1a-encoded nsps 2, 3 and 5 in the case of arteriviruses (Fig. 1), are known to play a critical role in RO formation. The three TMD-containing regions are conserved across nidoviruses and are referred to as TM1, TM2 and TM3 for simplicity hereafter. Previously, the expression of the TM1- and TM2-containing proteins (nsp2 and nsp3) of EAV was found to be sufficient to induce the formation of paired membranes and DMVs similar to those observed in infected cells (*47*). Subsequently, this was also observed for the TM1 and TM2-containing counterparts in coronaviruses (*116, 232*). The role of the TM3-containing subunits in DMV/RO biogenesis is less clear, but may

well be modulatory (*44, 48*). The ROs are believed to harbor the active viral replication and transcription complexes (RTCs) (*163*) and, in addition to modifying host cell endomembranes, TMD-containing nsps may serve to anchor other RTC components to RO membranes. For coronaviruses, DMVs have been identified as the main, if not only site of viral RNA synthesis (*61*). Abundant labeling of the DMV lumen for double-stranded (ds) RNA, an intermediate of viral RNA synthesis, strongly suggested nidovirus RNA synthesis to occur inside the DMVs (*55, 56, 62*). This would offer the advantage of an efficient compartmentalization of the RNA synthesis process and may also protect against the detection of dsRNA intermediates and minus-stranded RNA by cytosolic innate immune sensors (*233*). However, newly synthesized +RNA would need to cross the DMVs membranes to reach the cytosol for translation and packing into progeny virions. Our recent electron cryo-microscopy (cryo-EM) study of coronavirus ROs revealed a molecular pore that spans the two DMV membranes and thus appears to provide such a pathway from the DMV lumen to the cytosol (*234*). Furthermore, we could demonstrate that six copies of the large nsp3 make up the core of this potential RNA transport channel.

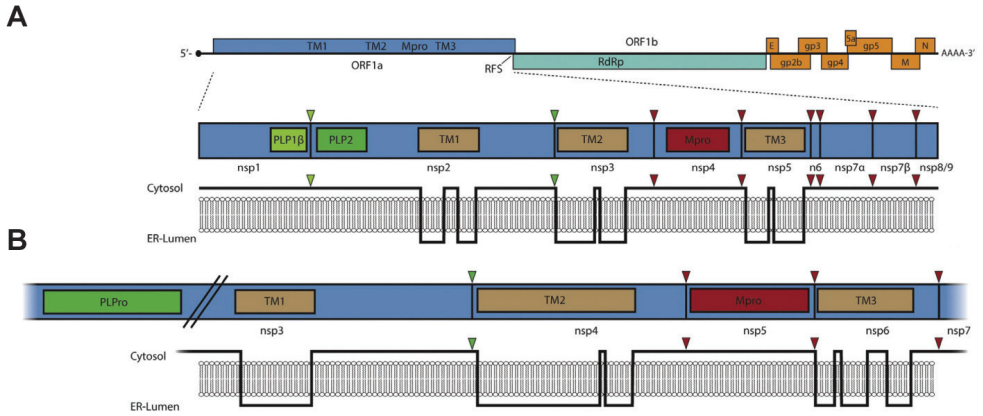

Figure 1. Schematic of the genome and nsp organization of arteriviruses. (A) Overview of the EAV genome organization (top). Important conserved domains encoded in ORF1a and ORF1b, such as the TMs, main proteinase (Mpro) and the RNA dependent RNA polymerase (RdRp) are indicated. The 3'-proximal quarter of the genome encodes structural protein genes (shown in orange), such as the viral glycoproteins (GP), envelope (E), membrane (M) and nucleocapsid (N) proteins. A scaled schematic of EAV pp1a is depicted in the middle panel, where three proteinases (papain-like proteinases 1β and 2 [PLP1β and PLP2, respectively] and Mpro) are indicated with colored boxes and their corresponding cleavage sites in pp1a with triangles. The bottom panel depicts the predicted membrane topology of the respective proteins. For comparison, a scaled schematic of the SARS-CoV pp1a (B) encompassing nsp3-7 is depicted (top). Nsp3 has been truncated to include the PLPro (green box) that cleaves the nsp3/4 junction. The bottom panel depicts the predicted the membrane topology the respective proteins. Adapted from (*48*)

Previous studies of the ultrastructure of arterivirus ROs made use of classical EM techniques comprising heavy-metal staining and resin embedding, which may induce structural artefacts. Moreover, the biological material was visualized only indirectly through the interacting stain, resulting in loss of macromolecular details. Here, we analyzed arterivirus ROs using cellular electron cryo-tomography (cryo-ET), which enables direct visualization of biological material in a close-to-native aqueous environment and thus preserves macromolecular details. This provided novel insights into the organization of arterivirus ROs, most importantly by revealing the presence of molecular pores that span the double membrane of arterivirus-induced DMVs. We could also show that the formation of such pores is independent of viral RNA synthesis, as they were found in cells expressing only subsets of the TMD-containing non-structural

proteins. Furthermore, we observed distinct RNP structures associated to the cytosolic side of the pores. This supports the hypothesis that the encapsidation of viral RNA exported from DMVs may occur in association with the cytosolic side of the pore, and is in line with similar observations made for coronavirus-induced DMVs (*234*). Our results demonstrate that the similarities in nidovirus ROs extend to molecular details such as the DMV-spanning molecular pores, which may be conserved across the *Nidovirales* order, highlighting their likely central role in the infectious cycle of these viruses.

Results

Morphology of arterivirus-induced ROs by cellular electron cryo-tomography

To analyze the structure of arterivirus-induced ROs in their native host cellular environment by cryo-ET, we examined MARC-145 or Huh7 cells infected with PRRSV or EAV, respectively. The infected cells were seeded on EM grids and cryo-fixed at advanced timepoints in infection, when ROs were highly abundant in the cytosol (*56, 57*). Subsequently, cryo-focused ion beam (FIB)-milling (*66*) was performed on the frozen-hydrated cells to generate 130-200 nm thin slices of vitrified intracellular material that were imaged by cryo-ET. For the ROs of both arteriviruses, the reconstructed tomographic data revealed reticulovesicular networks comprising DMVs and morphologically similar vesicles often containing two, but sometimes up to four inner vesicles sharing their outer membrane (Fig. 2). These structures, which had not been documented for arterivirus-infected cells thus far, were remarkably similar to the so-called vesicle packets (VPs) that were previously described in coronavirus-infected cells (*55, 234, 235*). VPs appeared to form during the later stages of coronavirus infection by the fusion of the outer membrane of multiple DMVs. For simplicity, arterivirus VPs will be considered a DMV subpopulation when discussed in the text hereafter. In general, and as previously reported (*48, 56*), arterivirus-induced DMVs, with average diameters of 116 and 151 nm (for EAV and PRRSV, respectively), were significantly smaller than coronavirus-induced DMVs, which are around 200-350 nm in diameter (*54, 55, 234, 235*). Variations in size were particularly apparent for PRRSV, where large DMVs, closer in size to coronavirus DMVs were often found, while EAV DMVs tended to be relatively small (Fig. 2C). Compared to previous studies on heavy-metal stained and resin-embedded samples (*48, 56*), the average DMV diameters were more than 20% larger, which could be a attributed to artefacts introduced in resin-embedded EM samples during preparation and imaging (*236*). The distance between the DMV inner and outer membrane appeared to be quite regular (about 4 nm spacing), resulting in a total thickness of ~13 nm for the double membrane. These observations match the double-membrane morphology found in coronavirus DMVs (*234*).

The majority of DMVs showed (neck-like) connections of their outer membrane with the ER and/or with other DMVs (Fig. 1). ER membranes could be found in close proximity of almost all DMVs in PRRSV- or EAV-infected cells. Free-floating DMVs, *i.e.* DMVs clearly devoid of membranous connections to ER or neighboring DMVs, were not detected in any of the data sets analyzed in this study. Similarly to previous studies on coronavirus-induced DMVs (*234, 235*), the DMV lumen was filled with filamentous structures, presumably containing dsRNA, but appeared to lack distinct proteinaceous assemblies. A few instances of zippered ER, which is presumed to be a precursor in DMV formation (*48, 115, 116, 237*), were found in data sets for both viruses (Fig. S1 A and D). Finally, DMVs with membrane openings were detected, though they were very rare (Fig. S1). In the EAV data set, one tomogram showed several curving double-membrane sheets originating from the same part of the ER (Fig S1 B and C), possibly documenting DMV formation as described earlier (*48*). These might

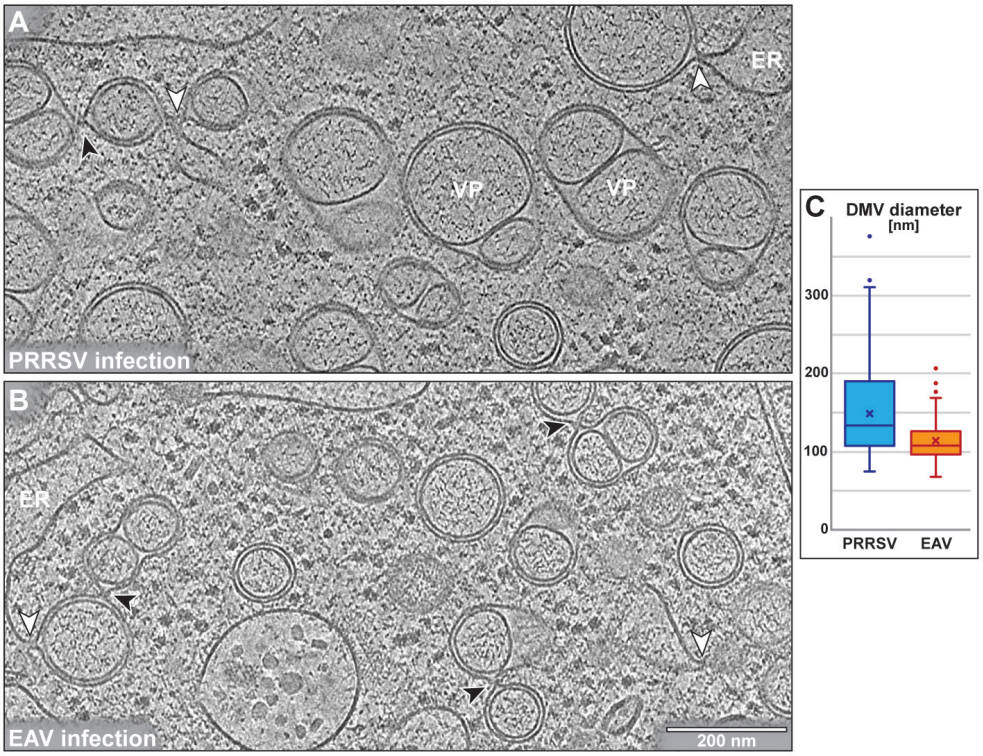

Figure 2. Replication organelles induced by PRRSV (A) and EAV (B) infection. Slices (7 nm thick) through the tomograms of cryo-lamellae from a (A) PRRSV-infected MARC-145 cell and (B) EAV-infected Huh-7 cell. Some vesicle packets (VP) and ER membranes (ER) are marked. ER-DMV and DMV-DMV neck-like outer membrane connections were frequently observed (white and black arrowheads, respectively) (C) Whisker-plots of the DMV diameters derived from both data sets (for PRRSV, n=374 from 24 tomograms of 6 individual cells; for EAV, n=116 from 4 tomograms of 3 individual cells). The crosses represent the average diameters, while outliers are represented as dots, see Materials & Methods for further details.

represent a final stage in DMV biogenesis, where the curving zippered membranes have not merged yet to form a sealed compartment. Some examples of membrane openings were also found in the PRRSV data set, in this case in VPs (Fig. S1 E and F), mostly suggesting that the VP had burst open on one side. In intact VPs, the inner vesicles appeared to be squeezed together, with their membrane interface being almost flat. In contrast, in disrupted VPs, the remaining intact inner vesicles were approximately spherical and appeared to push into the disrupted ones, which in response seemed to release their fibrillar content into the cytosol (Fig S1 E and F).

PRRSV- and EAV-induced DMVs contain double membrane-spanning molecular pores

Given our recent discovery of molecular pores in coronavirus-induced DMVs (*234*), we scrutinized arterivirus-induced DMVs for the presence of a similar structure. Strikingly, in both PRRSV- and EAV-induced ROs, pore complexes spanning the DMV double membrane were indeed detected (Fig. 3), although their dimensions were clearly much smaller. Unlike the coronaviral DMV pores, the DMV pores found in PRRSV- and EAV-infected samples did not feature distinct cytosolic 'crown-like' structures and smaller densities occasionally observed on the cytosolic side (Fig. 3 B and F, black arrowheads) did not seem to follow a regular

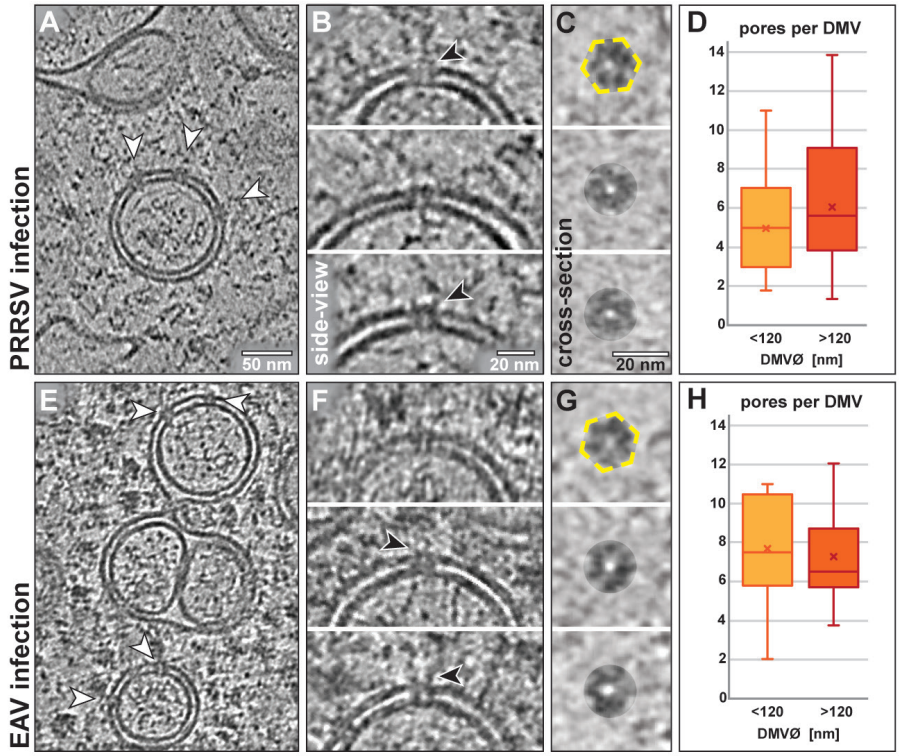

Figure 3: Molecular pores in PRRSV- (top) and EAV-induced (bottom) DMVs. (A, E) Overviews of arterivirus-induced DMVs that contain pore structures (white arrowheads) as present in PRRSV-infected cells (top) and EAV-infected cells (bottom). (B, F) Side-views of individual pore structures located around the equator of the DMVs, small densities associated to the cytosolic face of the complexes are indicated by black arrows. (C,G) Cross-sections of individual pores located in the top or bottom parts of the reconstructed DMVs. The section is taken halfway through the double membranes and thus corresponds to the inter-membrane platform of the pore. Examples of images suggesting a hexameric organization for the pore are marked by yellow dashed hexagons. Transparent circular masks with a diameter of 17 nm approximate the circumference of the pore complexes. (D, H) The numbers of pores identified in DMVs categorized as small (with a diameter of up to 120 nm) or large (diameter above 120 nm), does not differ drastically. For PRRSV, the average number of pores per DMV (crosses) was 4.9 and 6.2 for small and large DMVs, respectively (medians, 5.0 and 5.6 (central lines)). In the case of EAV, the average number of pores per DMV was 7.9 and 6.7 for small and large DMVs, respectively (medians, 7.8 and 6.3). For this analysis, seven tomograms of five individual cells were taken for PRRSV (resulting in 28 small and 33 large DMVs), and three tomograms of three individual cells for EAV (resulting in 14 small and 13 large DMVs).

pattern. In general, the pores consisted of a 17-18 nm-wide inter-membrane platform with a central channel that, about halfway through the double membranes, appeared to be ~3 nm wide (see cross-sections in Fig. 3C and G). For both EAV and PRRSV, the cross-sections along the central axis of those pores present in the top or bottom parts of the reconstructed DMVs did not show a consistent structure or symmetry, although some images appeared to suggest the presence of a hexamer (see Fig 3C and G, dashed yellow hexagons). Although the distinction of small macromolecular features in the inherently noisy cryo-ET data is limited, this suggests that arterivirus-induced DMV pores may be structurally heterogeneous. This may also be reflected by our thus far unsuccessful sub-tomogram averaging attempts, aiming to resolve the structure at higher resolution.

DMVs devoid of molecular pores were not present in our data. Our analyses suggest that the

number of pore structures per DMV does not substantially change with their size, with DMVs mostly containing 5 to 7 pores and pore numbers ranging from 2 to 14 in the DMVs analyzed for this study (Fig. 3D and H) (see Materials & Methods for details on the estimation of the number of pores).

Nucleocapsid and putative RNP assemblies are associated with the cytosolic side of DMV pores

In addition to the (double-) membrane structures in arterivirus-infected cells, the RO-containing regions also included a number of other macromolecular structures that are possibly linked to the process of RNA encapsidation and virus assembly. In the case of PRRSV, the cytosolic space surrounding RO membranes contained many roughly spherical protein shells of 35-45 nm diameter (Fig. 4A-C). About 18% of the identified DMV pores appeared to be associated with these protein shells (Fig. 4A, black arrowhead). Such structures were also present within envelope-containing virus particles (Fig. 4B and C), and therefore likely represent viral nucleocapsids. Their morphology and diameter of ~42 nm matched previous descriptions of nucleocapsids in purified PRRSV virions (*229*). Frequently, nucleocapsids were observed in association with smooth single-membrane vesicles, which could originate from ER or the Golgi apparatus (*238-240*) (Fig. 4C and D). There the nucleocapsids appeared to be enveloped by these membranes. Cytosolic nucleocapsids regularly appeared to colocalize near the virus budding sites and sometimes seemed to come in contact with each other (Fig 4E, white arrowhead).

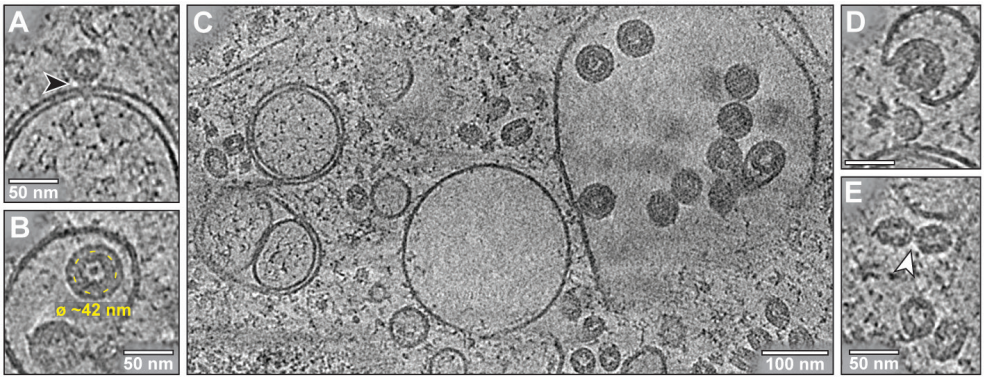

Figure 4. Nucleocapsids in PRRSV infection. In areas containing PRRSV-induced DMVs, (A) roughly spherical nucleocapsid structures were frequently observed, often associated with pore complexes in DMV membranes. (B,C) The nucleocapsids in virions were usually spherical with a diameter of ~42 nm. Such nucleocapsids were also found (D) in budding virions. (E) In the cytosol, nucleocapsids were often found in clusters in which individual capsids sometimes appear to come in contact (white arrowhead).

In the case of EAV-infected cells, similar roughly spherical nucleocapsids were present in the cytosolic space of RO-containing areas. Also association of nucleocapsids with DMV pores was regularly observed (Fig. 5A, black arrowhead). The cytosolic nucleocapsids resembled those present in virions within smooth-membrane organelles, which had a diameter of ~37 nm (Fig. 5B). However, cytosolic nucleocapsids were less abundant compared to PRRSV-infected cells, while two additional distinct macromolecular structures were present. The most prominent consisted of sheets that formed large and intertwined structures and frequently shaped into elongated tubes (Fig. 5C). Similar structures have been described in previous studies on EAV as well as for the arterivirus lactate-dehydrogenase elevating virus (LDV) (*56, 241, 242*). In the case of EAV, these sheets have been reported to label for N protein (*56, 242*), and to

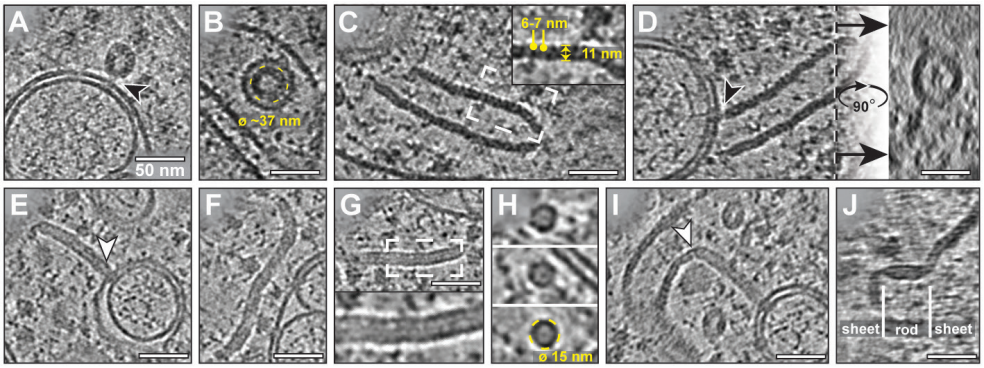

Figure 5. Nucleocapsids and putative RNP assemblies in EAV infection. (A) Cytosolic nucleocapsid structures were present in EAV RO regions, sometimes also found associated with molecular pores (black arrowhead). (B) An EAV particle within a membranous compartment showing a nucleocapsid diameter of about 37 nm. Next to roughly spherical nucleocapsids, (C) sheets that form larger assemblies were found in EAV-infected cells. The sheets were two-layered and about 11 nm wide, while each layer consisted of repeating molecular densities that show a 6-7 nm spacing. (D) The sheet structures sometimes appeared to associate with DMV molecular pores (black arrowhead), and often fold into tubular structures, which in cross-sections resembled viral nucleocapsids (a cross-section at the level of the vertical dashed line is depicted on the right). (E) Rod-like molecular structures were abundant in RO areas as well. These often appeared to originate from molecular pores, and extended into the cytosol perpendicularly from the DMV membranes. (F) The rod structures often bent to a certain extent and could reach lengths of more than 150 nm. XY tomographic slices along the rod axis (G) and in cross-section (H) both show a dense outer shell of ~15 nm diameter that shields a central filament, while regularly-spaced densities seem to connect the shell with the filament in each direction. (I) The rod structures often appeared continuous with the tubular sheets (white arrowhead) and (J), occasional they seemed to connect patches of sheet structures.

be absent when N protein expression is knocked out during infection (*238*). Additionally, it has been documented that overexpression of only the N protein is not sufficient to form these structures (*238*), which seem to have a high phosphate content (*56*). It was therefore hypothesized that these structures could be complexes of viral RNA and N protein. The macromolecular detail provided by our data supports this hypothesis. The sheets are double-layered and about 11 nm wide, with regular molecular densities that show a 6-7 nm spacing in each sheet layer. This pattern matches that of the previously described structure of arterivirus nucleocapsids (*229*), providing further evidence that they could be elaborate RNP assemblies. Occasionally, the sheets also seemed to interact with the molecular pores in DMV membranes.

The second distinct macromolecular structure found were rod-like filaments that frequently appeared to originate from molecular pores (Fig. 5E, white arrowhead). These rods sometimes exceeded lengths of 150 nm (Fig. 5F). In macromolecular terms, they consisted of a dense outer shell of about 15 nm diameter that appeared to shield a central filament (Fig, 5G and H). Small molecular densities, often regularly spaced, connected the central filament to the shell (Fig. 5G, inset). In some instances the rods were continuous with the tubular sheets (Fig, 5I), suggesting the possibility of a transformation of rods into sheets. We also found rod patches embedded in the sheet structures (Fig. 5J). Although the composition and function of both the sheet and rod structures are unclear, our data suggests that they could be different states of EAV RNP assemblies.

Regardless of their origin and (possible) role, it is striking that arterivirus nucleocapsids and potentially related structures were found to be associated with the cytosolic face of DMV pores, as also observed in coronavirus-infected cells (*234*). This suggests that, as previously

proposed, the pore could be a central hub for encapsidation of the exported RNA.

Arterivirus-induced DMV pores can form in the absence of viral RNA synthesis

To further investigate the requirements that have to be met to induce the formation of DMV pores, we also used cryo-ET to image cell lines expressing only a subset of EAV nsps, in particular those subunits previously implicated in the formation of DMVs (*48*). To this end, we used lentivirus-transduced Huh-7 cells stably expressing an EAV nsp2-7 polyprotein, which includes the three TMD-containing nsps (see Fig. 6A) and also the papain-like proteinase 2 (PLP2) domain in nsp2 and main proteinase (M^{pro}) domain in nsp4. In this system, the nsps up to nsp7 were included to generate the nsp5-7 processing intermediate that is particularly abundant in EAV-infected cells (*48, 243*) and to ensure the correct proteolytic cleavage of the polyprotein by the interplay of PLP2 and M^{pro}. This expression system, which does not direct arterivirus RNA synthesis as the ORF1b-encoded key enzymes required for this are lacking,

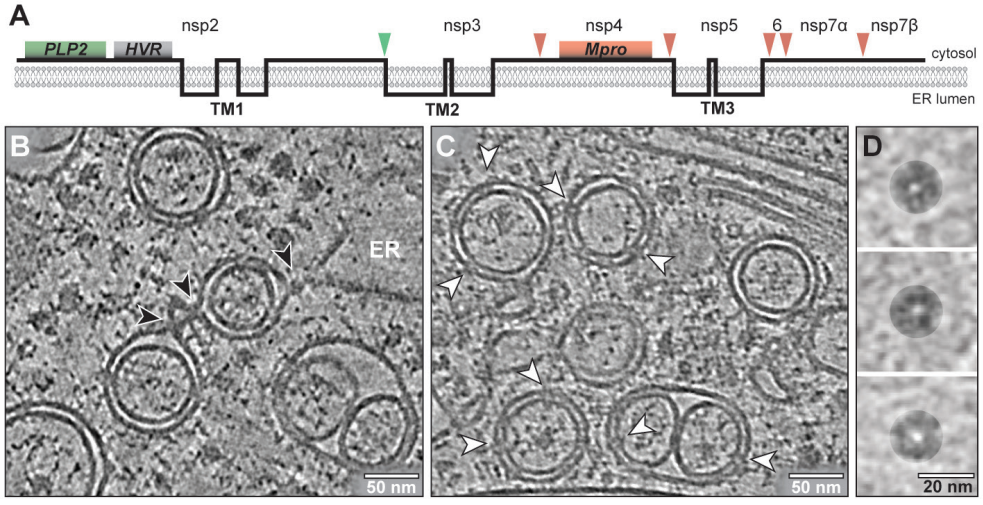

Figure 6. Pore complexes in DMVs induced by EAV nsp2-7 expression in Huh7 cells. (A) Presumed membrane topology of the expressed nsp2-7 polyprotein, with protease cleavage sites indicated by green (PLP2) and red (Mpro) arrowheads. The locations of the PLP2 and Mpro domains, as well as the hyper-variable region (HVR) of nsp2 are depicted by boxes. (B) Overall morphology of the nsp2-7-induced DMVs, which can also form VPs and establish neck-like outer membrane connections with other DMVs and with the ER (black arrowheads). (C) Pore structures (white arrowheads) were found embedded in the double membranes of the DMVs. These complexes resemble the pores found in DMVs induced by EAV infection (D), having a central channel and a similar diameter in cross-sections at the inter-membrane level.

was previously shown to generate DMVs similar to those observed in infected cells (*48*). In our present cellular cryo-ET analysis, the overall DMV morphology was strikingly similar to that in infected cell samples, as DMVs with perfectly spherical membranes and also vesicle packets were formed (Fig. 6B). Furthermore, the typical neck-like outer membrane connections to ER and neighboring DMVs were present (Fig. 6B, black arrowheads), while free-floating DMVs devoid of membrane connections were not observed. The nsp2-7-induced DMVs had a slightly smaller diameter compared to DMVs in EAV-infected cells (98 ± 15 nm, see Fig. 7), which is in line with previous observations (*48*). Other infection-related features, such as the fibrillar putative dsRNA content in the DMV lumen and structures potentially related to RNA encapsidation, were missing, as expected. Interestingly, our data revealed that also these

DMVs contained pore structures remarkably similar to those shown in Fig. 3. Although RTC components are absent in this system, these pore complexes seemed to be as abundant as the pores in the DMVs induced upon infection (Fig 6C). As far as the interpretation of the low-resolution data allows, the pore structures had the same general features as pore complexes in viral ROs in infected cells, with a diameter of about 17 nm and a central channel that was about 3 nm wide (Fig. 6D).

EAV nsp2 and nsp3 are sufficient to induce DMV and pore formation

The expression of a self-processing EAV nsp2-3 polyprotein was previously found to be sufficient for DMV formation (*47, 48*). We therefore analyzed whether this combination of TMD-containing proteins also suffices to form pores in the membranes of these DMVs, which showed substantial morphological differences compared to the DMVs formed upon expression of nsp2-7 or in EAV infected cells (Fig. 7A). Their membrane curvature was less regular, resulting often in oval DMVs (Fig. 7B). Putative intermediates of DMV formation, such as zippered ER or double-membrane sheets that appeared to be in the process of wrapping,

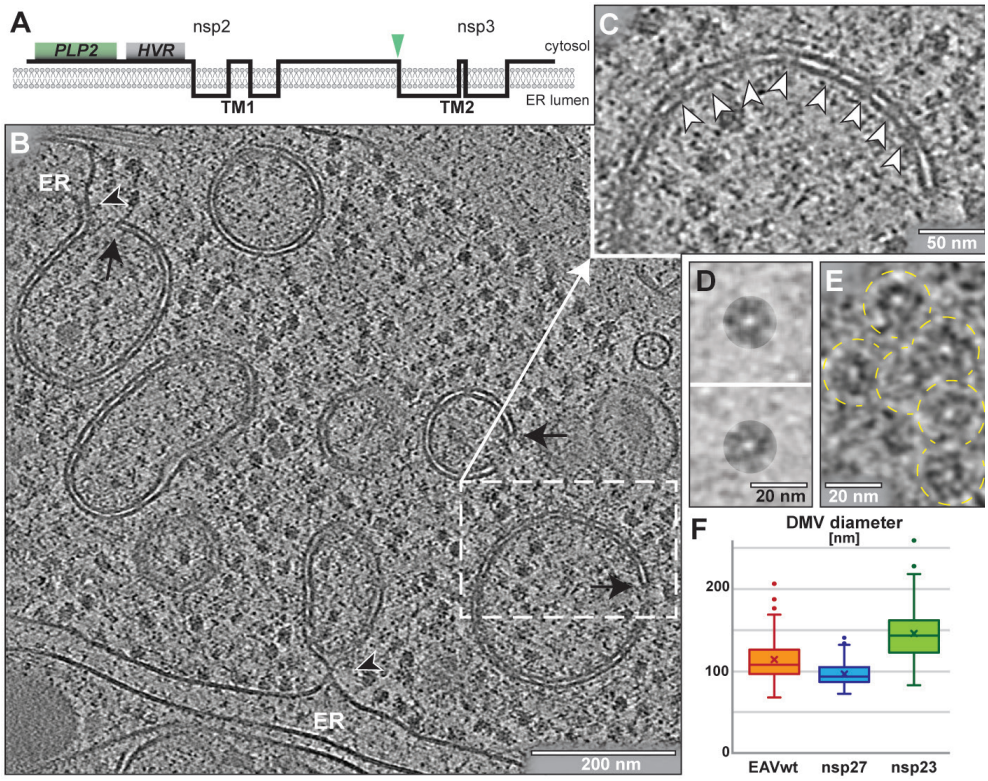

Figure 7. Pore complexes in DMVs induced by EAV nsp2-3 expression in Huh7 cells. (A) Presumed membrane topology of the nsp2-3 polyprotein, with the PLP2 domain, the HVR and the PLP2 cleavage site (green arrowhead) indicated. (B) Overview of DMVs showing irregular morphology, membrane openings (black arrows) and neck-like connections to the ER (black arrowheads). A close-up of the boxed area is presented in (C), showing a row of pore structures (white arrowheads) in a double membrane. (D) Cross-sections of the nsp2-3-induced pores highlighting the resemblance to pores in DMVs in EAV-infected cells (Fig. 2G). (E) Pore complexes were frequently observed in close proximity to each other, as depicted by this cross section of six individual complexes located on the top a DMV (outlined by dashed yellow circles). (F) Whisker plots comparing the diameter distributions of DMVs found in EAV-infected cells and the nsp2-7 and nsp2-3 polyprotein expression systems.

were frequently observed. In fact, membrane openings were found in the majority of DMVs. Moreover, VPs were not detected in our data. Taken together, all these characteristics suggests that DMV biogenesis was hampered in this nsp2-3 expression system. The average DMV diameter as well as the range of diameters observed were larger than upon EAV infection or nsp2-7 expression (Fig. 7F), which is consistent with previous results (*48*). Nevertheless, also in nsp2-3-induced DMVs pore structures were abundantly embedded in the double membranes. These again morphologically resembled the pores found in EAV-induced DMVs (Fig. 7C and D) with a central inter-membrane platform of ~17 nm diameter containing a channel of about 3 nm. The pore complexes were particularly abundant in this system, which was especially striking in larger DMVs, where they were frequently arranged in close proximity to each other (Fig. 7C and E).

Discussion

The formation of DMV pores is conserved between highly diverged nidoviruses

Replication organelles that support the viral RNA replication are a general feature in eukaryotic cells infected by +RNA viruses. The overall image that has emerged is that the RO membranes shield the ongoing viral RNA replication and its intermediates from cytosolic innate immune sensors, while newly synthesized RNA strands would be released to the cytosol for translation or to be packaged into virions. One of the typical RO morphologies are the invaginated spherules induced by some +RNA viruses, which exhibit open neck-like connections with the cytosol. In recent years, cryo-EM has helped to identify macromolecular channels at the neck-like membrane openings of such invaginations, which are likely involved in organizing viral RNA transport (*172, 244-246*). The other viral RO prototype consists of complex membrane networks comprising different virus-induced membrane structures, in which DMVs are a recurrent motif (reviewed in (*237*)). The DMVs induced by nidoviruses were initially characterized as lacking membrane openings that could facilitate a direct transport of molecules like RNA, but the discovery of the coronavirus DMV pore thanks to the use of cellular cryo-ET appeared to provide a solution to this transport riddle (*234*). To investigate whether such pores may be a conserved nidovirus feature, we now studied two arteriviruses, which are only distantly related to coronaviruses.

Despite the enormous evolutionary distance between arteri- and coronavirus replicases (*37, 119, 247*), their ROs evidently share major structural and functional features. These include the formation of a reticulovesicular network of modified (double) membrane structures and the generation of large numbers of DMVs. Our study extends these similarities to the presence of pore complexes that span the double membrane and thus provides a potential export route for viral RNA produced in the DMV lumen. Our findings suggest that the formation of pore-containing double-membrane compartments for viral RNA synthesis is a common feature of nidoviruses, a hypothesis that may now be explored for representatives of other families classified within this unique virus order.

Macromolecular organization and requirements for the formation of arterivirus DMV pores

An array of seven highly-conserved replicase domains has been proposed to constitute the core of the nidovirus RNA-synthesizing machinery (*6, 37*). In addition to the viral main protease (M^{pro}) and four ORF1b-encoded domains directly involved in viral RNA synthesis, this array includes two nsps with multi-spanning TMDs, namely TM2 and TM3, which flank the M^{pro} domain on either side (Fig. 1). An additional TMD (TM1) is present further upstream

in all nidovirus replicase polyproteins (*6, 37, 247*), although its position and features appear to have been less conserved during nidovirus evolution. In biological terms, the ROs of many nidovirus families remain fully uncharacterized so far, but our previous discovery of the TM1-containing coronavirus DMV pore (*234*) and the present data on arterivirus ROs strengthen the case to also consider TM1 part of the nidovirus core replicase. Our analysis of cells expressing only EAV nsp2-3 revealed that this combination of arterivirus nsps suffices to induce not only DMVs (*47, 125*) but also pores strongly resembling those found in DMVs in infected cells (Fig. 7). Likewise, co-expression of the TM1- and TM2-containing coronavirus replicase subunits induces DMV formation (*44, 116, 232*), although it remains to be established if these DMVs also contain pore structures.

As DMV pores appear to a conserved nidovirus feature, it is conceivable that also their macromolecular organization is similar, for instance using a common hexameric blueprint as suggested by some of our reconstructed arterivirus DMV pores (Fig. 3), which would be in line with the coronavirus DMV-spanning pore complex (*234*). However, despite the general similarities between arteri- and coronavirus nsps and DMVs outlined above, our results also unveiled striking differences: while the coronavirus-induced DMV pore features a large crown structure on its cytosolic side, such a structure is lacking in arterivirus-induced DMV pores and only small densities of irregular shape were occasionally observed. Assuming the coronavirus and arterivirus TM1-containing subunits are functionally equivalent and are core components of the DMV pore, this difference could be partially explained by the significantly smaller size of arterivirus nsp2. The arterivirus nsp2 region upstream of the TM1 domain only contains the PLP2 protease domain and a poorly characterized 'hypervariable region' (HVR) that is also the basis for the approximately two-fold size difference between EAV and PRRSV nsp2 (*228, 248*). The corresponding region of coronavirus nsp3 comprises about a dozen individual domains (*199*) with a combined molecular mass of ~160 kDa in the case of e.g. the murine hepatitis virus (MHV) or SARS-CoV-2. In coronavirus-infected cells, nsp3 was identified as the major component of the hexagonal DMV pore complex. The much smaller size of arterivirus nsp2 might have contributed to the limited detail that could be discerned for the arterivirus DMV pore structure in this study.

The apparently heterogeneous nature of the pore population found in arterivirus-induced DMVs suggests that the structure may also be highly dynamic. This may also explain our unsuccessful attempts to generate a higher-resolution model of the arterivirus DMV pore complexes by sub-tomogram averaging. Interestingly, the estimated resolution for the intermembrane platform of the MHV DMV pore obtained by subtomogram averaging was low relative to that obtained for the cytosolic crown (*234*). Taken together, these observations suggest that the inter-membrane platform of nidovirus DMV pores could be relatively dynamic.

For coronaviruses, six copies of nsp3 were not sufficient to account for the estimated mass of the DMV pore complexes (*234*), indicating that the molecular pore must contain other viral or host components. Our discovery of DMV pores in cells expressing only arterivirus nsp2 and nsp3 (Fig. 7) suggest that the TM2-containing subunit, which appears to be the primary interaction partner in arterivirus and coronavirus DMV formation (*45, 47, 48, 116*), could also be an integral part of the pore complex. Nonetheless, as this is only the second nidovirus DMV pore to be discovered, and given the absence of direct evidence for the presence or topology of the TM-containing proteins in the structure, it is important to leave space for alternative structural models. For example, although the TM3-containing subunit is apparently not

required for basic DMV and pore formation, this does not exclude the possibility that this protein could be a constituent of the pore in infected cells and has a role in its formation and/or function. Additionally, the presence of host factors cannot be excluded, underlining that the constituents of the pore complexes and the extent of the similarities across nidoviral DMV-spanning pores remain open questions that warrant further investigation.

Interestingly, the data from the EAV nsp2-3 and nsp2-7 expression systems revealed that the formation of a pore structure does not require the presence of RTC components, viral RNA or structural proteins. In recent cellular cryo-ET studies on coronavirus ROs (*234, 235*), distinct densities that might indicate the presence or location of RTCs inside the DMV lumen could not be identified. The same holds true for our data on arterivirus infection-induced DMVs. It is of note that the reliable detection of the relatively small molecular masses predicted for nidovirus RTCs (e.g. a proposed extended RTC complex of nsp7, 8, 9, 12 and 13 for SARS-CoV-2, ~ 300 kDa (*249*)) may not be possible in the cellular cryo-ET data due to the limited resolution (*250*), and likely contributes to the outcome of this analysis. Moreover, *in vitro* studies have identified enzyme complexes with different composition (*249, 251, 252*) that may coexist and perform different functions (*40*), which would further complicate their identification, particularly within the extensive fibrillar content of the DMVs. Thus, the search for the active nidovirus RTC at the cellular ROs remains an interesting challenge.

RO architecture and implications for DMV biogenesis

In general, the features of arterivirus ROs emerging from our data are in line with previous studies describing a large reticulovesicular network of interconnected DMVs originating from ER membranes (*48, 51, 55-57, 59, 234, 235*). We could not identify 'free-floating' DMVs that clearly lacked a connection to the surrounding ER or other DMVs, suggesting that fission of DMVs from the reticulovesicular network is not a common event in arterivirus-infected cells. It was striking, however, that the DMV populations found in our samples were dominated by a large fraction of VPs. This suggests and advanced stage in RO development, since it has been proposed for coronaviruses that VPs are the result of DMV fusion primarily happening at later stages of infection (*55*). The mechanism of nidoviral DMVs biogenesis is still unclear, although the results of different infection and nsp expression studies suggested a pathway in which zippered ER wraps into DMVs (*48, 115, 116, 237*). Aligning with previous observations, the low abundance of structures that may represent intermediates in DMV formation in our present data, provides further support for the hypothesis that that this process is rapid. In arterivirus-infected cells, we detected only a few instances of zippered ER and open DMVs (Fig. S1) that appeared to illustrate the proposed pathway to DMV formation. In contrast, these putative intermediate structures were extremely abundant in cells expressing nsp2-3. While the formation of DMVs in nsp2-3-expressing cells supports the crucial role of the TM1 and TM2 domains in the formation and organization of nidoviral ROs (*44, 47, 48, 116, 232*), our observations suggest that DMV formation is hampered. A comparison with the DMVs induced by EAV nsp2-7 expression (Fig. 6), suggests that the role in DMV formation of the nidovirus TM3-containing subunits (nsp5 in arteriviruses) could be of greater importance than previously anticipated. The nsp2-7-induced DMVs resembled much more closely the smaller and spherical DMVs found in infected cells, while also VP formation was observed (Fig. 2 and 6). The TM3-containing protein might modulate membrane curvature directly and/or by recruiting specific host proteins and/or lipids (*126, 253*), and thus could be a crucial factor for efficient DMV biogenesis.

The luminal content of the DMVs in expression systems strongly resembled the macromolecular landscape of the cytosol, while during arterivirus and coronavirus infection the DMV lumen was primarily occupied by putative (ds)RNA filaments ((*234, 235*) and this study). This suggests that the formation of DMVs encompasses the highly selective exclusion of cytosolic macromolecules, while primarily factors required for RNA synthesis might be enwrapped.

Molecular pores may coordinate viral RNA export from nidovirus induced DMVs with RNA encapsidation

Although the presence of molecular pores in the DMV membranes can be taken to suggest viral RNA transport across the double membrane, direct evidence for this hypothesis or mechanistic insights into the function of DMV pore complexes are still lacking. In coronavirus-infected cells, RNPs were abundantly detected near DMVs, sometimes in contact with the DMV-pore (*234*). This led to a model in which the DMV-spanning pores would coordinate RNA export and encapsidation. A similar model is strongly supported by our current data from PRRSV- and EAV-infected cells. Nucleocapsid-like structures were frequently found to have direct contact with DMV pores, suggesting rapid encapsidation of exported viral genomic RNA (Fig. 4 and 5). Although the exact role and nature of the additional putative RNP structures observed in our data from EAV-infected cells remain to be established, it is interesting to note that these structures also seem to interact with the DMV pore (Fig. 4 and 5), further aligning with this model.

Only a fraction of the synthesized +RNAs generated by the nidoviral RTCs are full length gRNAs that could be packaged into progeny virus particles. In fact, the vast majority of +RNA transcripts synthesized are sg-mRNAs to be translated into viral structural or accessory proteins. These sg-mRNAs, presumably also are exported through the molecular pore, would not require encapsidation, which also holds true for gRNAs translated into additional replicase polyproteins. Such RNA strands would likely not be reliably detectable in the crowded cytosol in our cryo-ET data. Yet the majority of the identified pore complexes in PRRSV-induced DMVs (more than 80%) were not associated with nucleocapsid structures. It could be speculated that this subset of pores is involved in the export of viral sg-mRNA strands. In this scenario only gRNAs to be packaged into virions would be encapsidated by the cytosolic N-protein, a process that might be coordinated by the pore complex. The molecular basis for this role of the DMV pore in nidovirus-infected cells could be the reported interaction of the TM1-containing subunit with N protein (*202, 203, 254*). Our combined observations in PRRSV-infected cells support a pathway of gRNA encapsidation at the pores followed by budding into the lumen of smooth ER or Golgi membranes (Fig. 4).

In summary, our study shows that DMVs molecular pores are a conserved feature of nidovirus replication that likely serve as central hubs in the nidoviral replication cycle by connecting viral RNA synthesis with encapsidation. This central role makes these newly-discovered macromolecular complexes attractive targets for antiviral therapies.

Materials and methods

Virus infections

For PRRSV infection MARC-145 cells were maintained at 37 ˚C and 5% CO_2 in Dulbecco's modified Eagle's medium (DMEM) supplemented with 8% fetal bovine serum (FBS), 100 U/mL penicillin, and 100 µg/mL streptomycin. Cells were seeded at a density of 4×10^4 cells per cm^2 in cell culture dishes (Greiner Bio-One). Three days after seeding, cells reached full confluency, a state in which they are most susceptible for PRRSV infection. Cells were infected with genotype 1 PRRSV isolate SD01-08 [GenBank accession #DQ489311; (*255*)] at an MOI of 2 and incubated at 37 ˚C Since confluent cell layers have a too large cohesive mass for proper vitrification of all cellular material by plunge freezing, we trypsinized the infected cells at 17 h p.i., diluted them 1:10 in cell culture medium and seeded them again in 10 cm^2 cell culture dishes containing EM grids. At 24 h p.i. cells were cryo-immobilized for analysis.

For EAV infection, Huh-7 cells were maintained as described previously (*48*). 16 h prior to infection cells were seeded at a density of 1×10^4 cells per cm^2 in cell culture dishes containing EM grids and subsequently incubated at 37 ˚C. Cells were infected with a cell-culture adapted derivative of the EAV Bucyrus isolate (*23*) at an MOI of 50 and incubated at 39.5 ˚C thereafter. At 9 h p.i., cells were cryo-immobilized for analysis.

Cell lines stably expressing EAV nsps

Lentivirus-transduced HuH-7 cell lines expressing EAV nsp2-nsp3 or nsp2-nsp7 (*48*) were cultured in selection medium containing 500 µg/ml G418 (PAA Laboratories) and 12.5 µg/ml Blasticidin-S (PAA Laboratories). Seven hours prior to induction cells were seeded at a density of 8×10^3 cells per cm^2 in cell culture dishes containing EM grids. Expression of EAV nsps was induced for 24 hours using 1 µg/ml tetracycline (Invitrogen) before cryo-immobilization for analysis.

EM sample preparation for cellular electron cryo-tomography

R1/4 gold Quantifoil grids (200 mesh, Quantifoil Micro Tools) were cleaned overnight on a chloroform-soaked filter paper in a sealed glass dish. Dried off grids were glow-discharged and placed in 10 cm^2 cell culture dishes containing PBS and UV-sterilized for 30 min in a laminar flow cabinet. PBS was removed and cells were seeded at the respective densities and maintained accordingly. For cryo-fixation, grids were plunge-frozen in liquid ethane with a Leica EM GP automated plunge-freezer (Leica Microsystems), after applying 10 s of blotting from the backside of the grid and 1 s post-blotting time in conditions of 95% humidity and 37 °C or 39 °C , for EAV or PRRSV samples, respectively. Grids were stored in liquid nitrogen until further processing. For cryo-lamella preparation grids were transferred to an Aquilos cryo-focused ion beam scanning electron microscope (FIB-SEM) (Thermo Fisher Scientific) and cryo-lamellae were generated as described previously (*214*).

Cellular electron cryo-tomography

Tilt-series acquisition was performed using Titan Krios (Thermo Fisher Scientific) electron microscopes operated at 300 kV and equipped with a Gatan BioQuantum energy filter (Gatan) and either a Gatan K3 or Gatan K2 summit direct detection device, the latter being used for part of the EAV infection data. Movie frames were collected in counting mode at zero-loss imaging with a 20-eV slit width. The pixel size was 3.28 Å (K3 data) or 3.51 Å (K2 data) and defocus values ranged from -4 to -8 µm. Dose-symmetric tilt series (*215*) were collected with

serialEM software (*256*), while bi-directional tilt series were collected with FEI Tomo4 (K2 data). The total dose applied on the sample was 120-140 $e^{-}/Å^{2}$, which was distributed over tilt series covering a 100˚- 120˚ range with 2 or 3˚ tilt increments. The amount of high-quality tilt series collected and used for analysis were: 34 for PRRSV infection, 33 for EAV infection (20 collected on the K3, 13 on the K2 data), 20 for EAV nsp2-nsp3 expression, 6 for EAV nsp2-nsp7 expression.

Tomographic data processing

Recorded movie frames were aligned with MotionCor2 using 5 x 5 patches (*188*). The resulting fiducial-less tilt-series were aligned and reconstructed with AreTomo v1.0.10 (*257*). For alignment, global and local alignment was applied using 7 x 5 patches on full-sized K3 images and 5 x 5 patches for K2 data. The number of patches was accordingly reduced in some tilt-series that had been cropped to remove contaminations from the field of view. Tomograms were reconstructed using SART (Simultaneous Algebraic Reconstruction Technique) with 20 iterations and 5 projections per iteration. CTF-estimation was done on the aligned tilt-series with ctffind4 (*216*), while CTF-correction and denoising for visualization and modelling purposes was carried out using ctfphaseflip (*217*) and the nonlinear anisotropic diffusion (*218*) packages included in IMOD (*219*).

Data analysis and statistics

Individual DMV pore complexes as well as the DMV centers were annotated on the tomograms using the model option in IMOD (*219*). For the center of the DMV, the central point at the level of the DMV equator was selected, while the pore positions were placed in the center of the inter-membrane platform. These coordinates were then extracted and used for the quantifications of DMV sizes and number or pores per DMV. The average of the distances of all the pores in a DMV to the corresponding DMV center was calculated, and considered to be the DMV radius after adding 6.5 nm to account for the distance of the pore center to the DMV cytosolic face of the outer DMV membrane. In the case of EAV nsp2-3 expression, only DMVs showing a roughly spherical morphology were included in the statistics. To estimate the number of pores per DMVs, we took into account that not all DMVs were fully reconstructed in the cryo-tomograms due to the removal of biological material during cryo-lamella milling. In these cases, we assumed that (I) a DMV is spherical and (II) that the average pore density is constant across the whole DMV surface. Using these assumptions, we determined the percentages of DMV surface area that was contained in the cryo-lamella and extrapolated the number of pores detected in this region to the full DMV surface. Even though VPs contained abundant molecular pores, for simplicity, no vesicle packets were included in this calculation.

In all the whisker-plots presented in this work, the bottom and top boxes of the plot represent the second and third quartile, respectively. The whiskers extend to the minimum and maximum values measured, while outliers that exceeded Q2 or Q3 by a distance of 1.5 times the interquartile range are depicted as dots. Outliers were included in the calculation of the medians (middle lines) and averages (crosses).

Acknowledgements

We are grateful to Ying Fang (Department of Pathobiology, College of Veterinary Medicine, University of Illinois, Urbana, USA) for providing the PRRSV isolate and helpful discussions, Diede Oudshoorn and Marjolein Kikkert for the EAV nsp-expressing cell lines and Jessika Zevenhoven-Dobbe, Linda Boomaars-van der Zanden, Emmely Treffers and all other colleagues of the LUMC Molecular Virology group that provided help and assistance. We thank Frank Faas for technical support and Shawn Zheng (Dept. Biochemistry and Biophysics, University of California, San Francisco, USA) for the continuous support and helpful discussions about the processing of cryo-ET data, which was collected at the Netherlands Centre for Electron Nanoscopy (NeCEN) with assistance from Wen Yang, Christoph Diebolder and Ludovic Renault. Access to NeCEN was made possible through financial support from the Dutch Roadmap Grant NEMI (NWO grant 184.034.014).

Supplementary figure

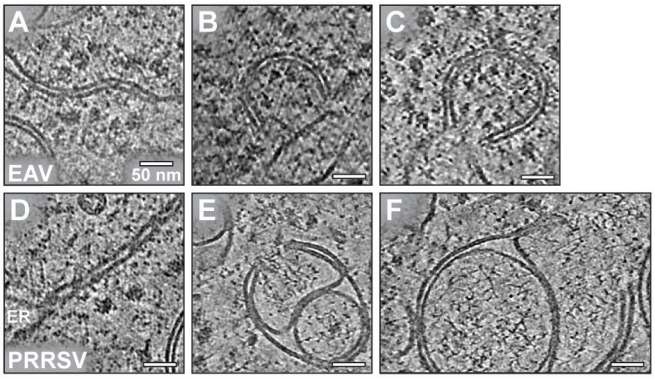

Figure S1. Putative intermediates in DMV formation and double-membrane openings. Replication organelle elements representing putative intermediates in DMV formation are present EAV-infected cells (top): (A) zippered ER membranes, that sometimes appear to (B) curve and (C) wrap up into a non-sealed DMV. (D) Zippered ER membranes were also present in PRRSV data, where additionally (E, F) double-membrane openings were found in vesicle packets that appeared to have burst open.

CONSERVATION OF A DOUBLE-MEMBRANE SPANNING MOLECULAR PORE IN THE REPLICATION ORGANELLES OF DISTANTLY-RELATED NIDOVIRUSES